NASA/TM-20205011621

Micromechanics Modeling of Textiles for Re-Entry Parachute Applications

Brandon L. Hearley
North Carolina State University, Raleigh, North Carolina

Evan J. Pineda and Brett A. Bednarcyk
Glenn Research Center, Cleveland, Ohio

Scott M. Murman
Ames Research Center, Moffett Field, California

Mark Pankow
North Carolina State University, Raleigh, North Carolina

January 2021

NASA STI Program . . . in Profile

Since its founding, NASA has been dedicated to the advancement of aeronautics and space science. The NASA Scientific and Technical Information (STI) Program plays a key part in helping NASA maintain this important role.

The NASA STI Program operates under the auspices of the Agency Chief Information Officer. It collects, organizes, provides for archiving, and disseminates NASA's STI. The NASA STI Program provides access to the NASA Technical Report Server—Registered (NTRS Reg) and NASA Technical Report Server—Public (NTRS) thus providing one of the largest collections of aeronautical and space science STI in the world. Results are published in both non-NASA channels and by NASA in the NASA STI Report Series, which includes the following report types:

- TECHNICAL PUBLICATION. Reports of completed research or a major significant phase of research that present the results of NASA programs and include extensive data or theoretical analysis. Includes compilations of significant scientific and technical data and information deemed to be of continuing reference value. NASA counter-part of peer-reviewed formal professional papers, but has less stringent limitations on manuscript length and extent of graphic presentations.

- TECHNICAL MEMORANDUM. Scientific and technical findings that are preliminary or of specialized interest, e.g., "quick-release" reports, working papers, and bibliographies that contain minimal annotation. Does not contain extensive analysis.

- CONTRACTOR REPORT. Scientific and technical findings by NASA-sponsored contractors and grantees.

- CONFERENCE PUBLICATION. Collected papers from scientific and technical conferences, symposia, seminars, or other meetings sponsored or co-sponsored by NASA.

- SPECIAL PUBLICATION. Scientific, technical, or historical information from NASA programs, projects, and missions, often concerned with subjects having substantial public interest.

- TECHNICAL TRANSLATION. English-language translations of foreign scientific and technical material pertinent to NASA's mission.

For more information about the NASA STI program, see the following:

- Access the NASA STI program home page at http://www.sti.nasa.gov

- E-mail your question to help@sti.nasa.gov

- Fax your question to the NASA STI Information Desk at 757-864-6500

- Telephone the NASA STI Information Desk at 757-864-9658

- Write to:
  NASA STI Program
  Mail Stop 148
  NASA Langley Research Center
  Hampton, VA 23681-2199

NASA/TM-20205011621

Micromechanics Modeling of Textiles for Re-Entry Parachute Applications

Brandon L. Hearley
North Carolina State University, Raleigh, North Carolina

Evan J. Pineda and Brett A. Bednarcyk
Glenn Research Center, Cleveland, Ohio

Scott M. Murman
Ames Research Center, Moffett Field, California

Mark Pankow
North Carolina State University, Raleigh, North Carolina

National Aeronautics and
Space Administration

Glenn Research Center
Cleveland, Ohio 44135

January 2021

Acknowledgments

The authors would like to thank the NASA Space Technology Mission Directorate (STMD) Entry Systems Modeling (ESM) project, the Aeronautics Research Mission Directorate (ARMD) Transformational Tools and Technologies project and the Lewis' Educational and Research Collaborative Internship Project (LERCIP) for their support of this work.

Level of Review: This material has been technically reviewed by technical management.

Available from

NASA STI Program
Mail Stop 148
NASA Langley Research Center
Hampton, VA 23681-2199

National Technical Information Service
5285 Port Royal Road
Springfield, VA 22161
703-605-6000

This report is available in electronic form at http://www.sti.nasa.gov/ and http://ntrs.nasa.gov/

Micromechanics Modeling of Textiles for Re-Entry Parachute Applications

Brandon L. Hearley*
North Carolina State University
Raleigh, North Carolina 27695

Evan J. Pineda and Brett A. Bednarcyk
National Aeronautics and Space Administration
Glenn Research Center
Cleveland, Ohio 44135

Scott M. Murman
National Aeronautics and Space Administration
Ames Research Center
Moffett Field, California 94035

Mark Pankow
North Carolina State University
Raleigh, North Carolina 27695

Abstract

Recent flight test projects and NASA missions have highlighted the challenges associated with accurately and efficiently modeling the behavior of parachute deployment systems needed for parachute design. Moreover, parachute deployment has been identified as one of the higher risk components for such missions. The analysis of textile fabrics used for atmospheric entry is inherently complex due to the multiple scales present in the fabric structure, including individual fiber filaments at the microscale, yarn bundles of fibers at the mesoscale, and the overall woven fabric at the macroscale. Computational tools for simulating fabric behavior must be able to account for the different mechanisms present at each scale without sacrificing computational efficiency. This work applies the generalized multiscale method of cells micromechanics theory, which has previously been used for the analysis of reinforced composite structures, to unreinforced textile fabrics. Modifications to the existing composite multiscale framework, implemented in NASA's Multiscale Analysis Tool (NASMAT), include the specific mechanics unique to unreinforced textile fabrics, and overcoming the assumptions of a fixed fiber angle. This study assesses the feasibility of using the NASMAT tool for efficient prediction of the response of unreinforced fabrics to loading such that it can ultimately be applied to fluid structure interaction tools for the prediction of parachute deployment systems. Fabric behavior is simulated in NASMAT through homogenization of a triply periodic repeating unit cell, where the geometry of the subcells can change as a function of loading to represent the relative rotation and uncrimping that can occur in fabric tows. Predictions from the amended NASMAT code are compared to experimental data for uniaxial and off-axis tension to verify the ability of the code to incorporate lower-scale mechanics in prediction of unreinforced fabrics under loading.

*Summer Intern in Lewis' Educational and Research Collaborative Internship Project (LERCIP).

Nomenclature

a	Contact radius
A	cross-section area
b	uncrimping rate
C	stiffness matrix
d	distance
L	sample length
E	modulus of elasticity
F	Contact force
g	interface stiffness scaling parameter
G	shear modulus
P	pressure at tow cross-over
Q	orthogonal transformation matrix
r	radius of tow half lens
R	tow radius of effective sphere
S	compliance matrix
T	nonorthogonal transformation matrix
V_f	tow volume fraction
W	sample width
γ	shear strain
δ	displacement
ε	strain
η	off-axis loading angle
θ	tow rotation angle
μ	interface subcell relative width
ν	Poisson's ratio
σ	axial stress
τ	shear stress
ϕ	tow crimp angle

Introduction

Parachute deployment systems often carry high risk for space and flight missions due to the complexity and number of moving parts associated with these systems and their dependency on timing and staging. The materials used for parachutes are also inherently complex due to the multiple scales that are present within the parachute's fabric structure. Materials used for parachute deployment systems consist of microscale fiber filaments bundled together to produce mesoscale yarns, which are interwoven to produce the macroscale fabric. The analysis used for the design of parachute systems and materials is also heavily reliant on legacy data, making it difficult to accurately and efficiently implement new materials that can aid in design and reduce risk. It is therefore desirable to develop computational models that can predict the overall behavior of these fabrics and the mechanics that occur at lower scales while avoiding the computational inefficiency of high-fidelity models.

The behavior of unreinforced textile fabrics has been studied and modeled with continuum mechanics at the various scales present in the fabric's structure. Microscale models, whose elements represent the individual filaments that make up the yarns or tows of a fabric, have the advantage of explicitly modeling

specific mechanics that occur at the microscale, but suffer from computational inefficiency due to the high number of elements required for discretization, often making them too expensive to use for real-world structures (Refs. 1 to 3). To improve on the efficiency of fabric models, researchers have widely implemented mesoscale models, in which the yarns within the fabric are modeled with orthotropic elastic properties (Refs. 4 to 6). These models alleviate computational cost but lose information of the mechanics at the microscale and can require nonlinear material models in their formulation. Computational cost can be further reduced with macroscale models, which look to simulate overall fabric behavior through homogenized material properties that effectively incorporate the mechanics that occur at lower scales (Refs. 7 and 8). Though the existing models for textile fabrics are able to predict macrolevel response to loading, they and often rely on experimental testing of the fabric as inputs to the material model and use of empirical factors, limiting the predictive capabilities of such simulations.

Computational cost and the lack of information at lower scales has be addressed through multiscale modeling, in which material properties are defined at lower scales and information is passed back and forth between scales through homogenization and localization techniques. Nilakanten et al. implemented a multiscale model for simulating the ballistic impact response of Kevlar fabric by incorporating different scales, and levels of fidelity at different regions in the model, to improve computational time (Ref. 9). The model featured solid-element discretization of the mesoscale yarns at the region of impact, developed hybrid woven shell elements modeling the mesoscale yarns near the impact region, and low fidelity homogenized shell elements far from impact, and was able to show that a multiscale model can significantly improve computational time without sacrificing accuracy in prediction of the fabric macroscale behavior. Verpoest and Lomov developed the *WiseTex* software, which is capable of performing multiscale analysis of textile fabrics and composites on a unit cell level, including predictions of structural behavior, fabric permeability, and fabric drapeability, by use of Eshelby's method of inclusions for subdivisions within a fabric repeating unit cell (RUC) (Ref. 10). Lomov et al. further showed that damage can be simulated in the multiscale model by defining damage criteria at the microscale and, by passing information between scales, applying it to elements at higher scales through degradation of the stiffness matrix (Ref. 11).

Another integrated multiscale tool that has been shown to predict the behavior of composite structures is NASA's Multiscale Analysis Tool (NASMAT), which was developed from NASA's Micromechanics Analysis Code with Generalized Method of Cells (MAC/GMC) developed at the NASA Glenn Research Center. Bednarcyk showed that MAC/GMC is able to predict the elastic properties of polymer matrix composites (PMC) for arbitrary woven and braided reinforced fabrics (Ref. 12). Bednarcyk and Arnold extended the MAC/GMC code to allow for modeling of damage modes at the microscale, such as fiber breakage, showing the capabilities of the multiscale tool to predict damage at the higher scales (Ref. 13). Ricks et al. studied the tool's ability to predict the material properties of 3D woven textile composites, showing good agreement between the tool and finite element (FE) techniques for in-plane properties (Ref. 14). Liu et al. showed that a generalized multiscale GMC methodology can be used for efficient analysis of textile composites (Ref. 15). Through homogenization and localization procedures outlined between the micro, meso, and macroscale, the developed modeling technique was able to predict elastic moduli and transverse tensile failure of triaxially braided composites.

NASMAT uses a three-dimensional triply periodic repeating unit cell (RUC) version of GMC, originally developed by Aboudi (Ref. 16), implementing constituent material properties (fiber and matrix) at the microscale, allowing for an efficient homogenization procedure for PMCs. Using a micromechanics approach with constituent material properties as an input, NASMAT is able to predict the average macroscale behavior of a composite and provide microscale information within the RUC. GMC is advantageous compared to other micromechanics theories due to its fully multi-axial formulation, availability of constituent level stress and strain fields, and its computational efficiency (Ref. 17).

NASMAT has proven its ability to predict nonlinear behavior of composite materials in a time effective manner through an integrated multiscale recursive approach. However, in its current formulation it is limited to reinforced fabric structures due to its assumptions of fixed fiber orientations throughout analysis and the presence of two microscale constituents, i.e., a fiber and matrix. For unreinforced fabrics, no matrix material is present, which allows tows to rotate and change shape with applied loading. The aim of this work is to assess the feasibility of using the NASMAT tool for efficient prediction of the deformational response of unreinforced fabrics to mechanical loads, such that it can ultimately be applied to fluid structure interaction tools for the prediction of parachute deployment systems. It looks to address the assumptions of fixed fiber orientation by capturing the mechanics that occur at lower scales and incorporating tow movement into each subcell of the RUC in the homogenization procedure. Tow interaction is modeled through fictitious interface subcells in the RUC with properties dependent on a Hertzian contact theory. The results of the amended NASMAT code for unreinforced textile fabrics are then compared to experimental data from the literature for uniaxial tension and off-axis tension cases for verification.

Method

Repeating Unit Cell

Homogenization of a plain weave fabric is accomplished through analysis of a representative volume element (RVE) of the mesoscale structure, which contains two warp yarns and two weft yarns (Figure 1). In NASMAT, the RVE is represented by a triple periodic RUC, which features four subcells in the warp (1) direction, four subcells in the weft (2) direction, and two subcells in the thickness (3) direction, shown in Figure 2. A single tow within the repeating unit cell is represented by four subcells along its length and two for its cross-section. The orientation of the fibers within a subcell are characterized by two angles, ϕ_{warp} and θ_{warp} for warp yarns and ϕ_{weft} and θ_{weft} for weft yarns, where ϕ represents the tow crimp angle, or angle of undulation of the tow, and θ represents the tow rotation angle relative to its initial orientation.

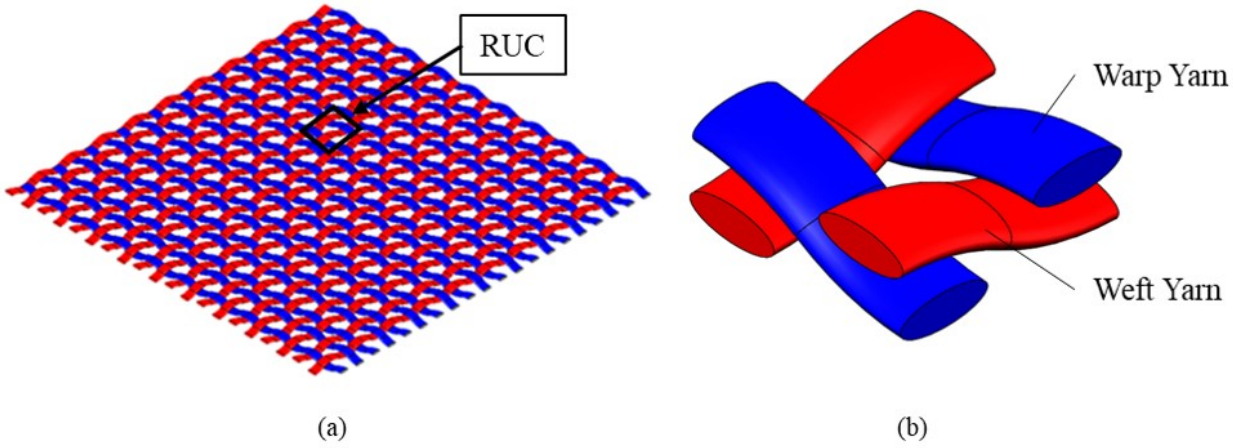

Figure 1.—(a) Plain Weave Fabric and (b) Representative Repeating Unit Cell (RUC).

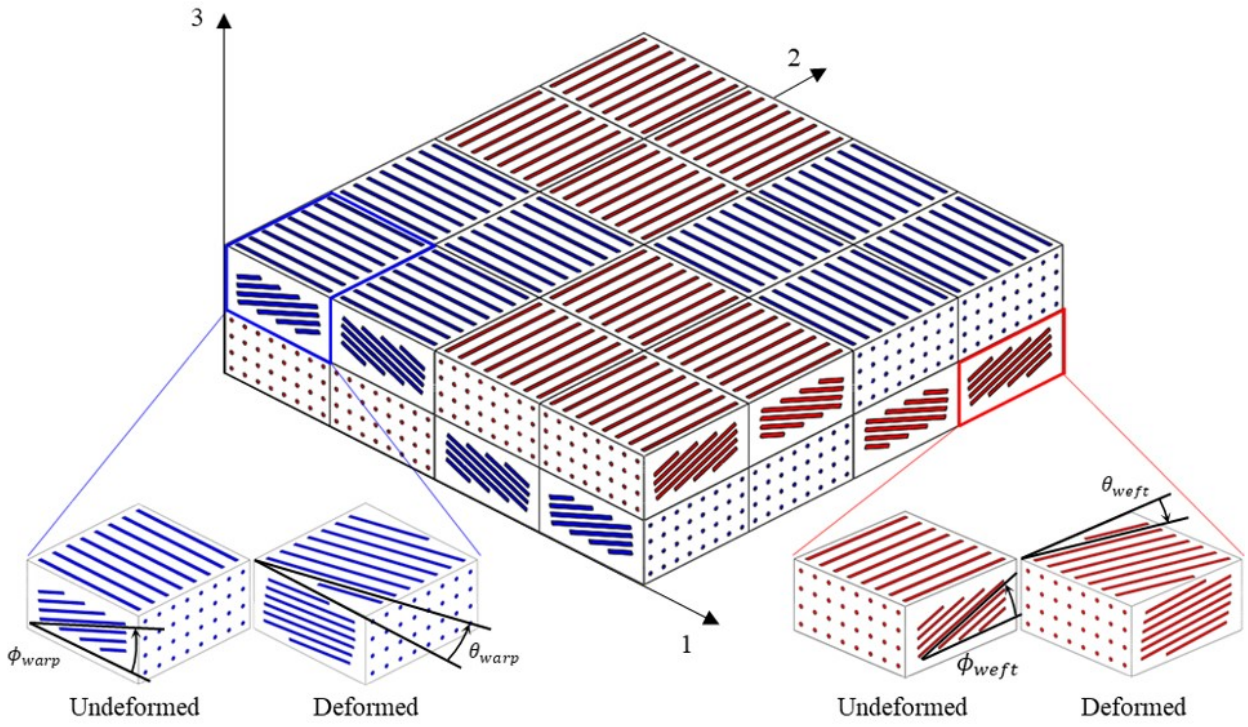

Figure 2.—Triply Periodic Repeating Unit Cell of Plain Weave Fabric.

At any given load step, it is assumed that the each yarn is in a uniform state, such that all subcells representing warp yarns will have the same value of θ_{warp} and $|\phi_{warp}|$ and all subcells representing weft yarns will have the same value of θ_{weft} and $|\phi_{weft}|$. Crimp angles can be either positive or negative, allowing each subcell to be defined by one of four orientations at each load step. Subcells are modeled with orthotropic mesoscale (yarn-level) material properties. In the yarn's coordinate system, where the 1-axis is aligned with the axial direction of the yarn, its compliance and stiffness matrices are defined as

$$S_{yarn} = \begin{bmatrix} \frac{1}{E_A} & -\frac{\nu_{21}}{E_T} & -\frac{\nu_{31}}{E_T} & 0 & 0 & 0 \\ -\frac{\nu_{12}}{E_A} & \frac{1}{E_T} & -\frac{\nu_{32}}{E_T} & 0 & 0 & 0 \\ -\frac{\nu_{13}}{E_A} & -\frac{\nu_{23}}{E_T} & \frac{1}{E_T} & 0 & 0 & 0 \\ 0 & 0 & 0 & \frac{1}{2G_{12}} & 0 & 0 \\ 0 & 0 & 0 & 0 & \frac{1}{2G_{13}} & 0 \\ 0 & 0 & 0 & 0 & 0 & \frac{1}{2G_{23}} \end{bmatrix} \tag{1}$$

$$C_{yarn} = S_{yarn}^{-1} \tag{2}$$

In the global coordinate system, each subcell's stiffness matrix is rotated by converting it to a 4th order tensor, rotating the tensor by ϕ and θ, and converting back to a 6×6 matrix. To obtain a single stiffness matrix for the fabric a two-step homogenization procedure is used in GMC (Refs. 15 and 17). In the first step, subcells are homogenized through the thickness at each location in the 1-2 plane, resulting in an intermediate repeating unit cell with four subcells in the 1 and 2 direction and only one in the 3 direction. Eight unique through-the-thickness groups can be identified in the original RUC, which each appear twice in the intermediate RUC (Figure 3).

In the second step, the fabric RUC is homogenized using the eight group stiffness matrices. The two-step process is required due to the discontinuous path of a tow within the RUC, shown in Figure 4, and the lack of normal and shear coupling in References 16 and 18. Without using the two-step procedure outlined, GMC has been shown to severely underpredict in-plane stiffness (Ref. 18).

Each tow's cross-section is represented by two rectangular subcells in the RUC, but physically tow shapes are often best represented by lenses or ellipses. For reinforced composites, the presence of a matrix surrounding the fibers and the application of unidirectional composite material properties to the individual subcells allows the rectangular representation of the cross-section to be accurate. In a similar fashion for an unreinforced fabric, a rule of mixtures with zero-stiffness "air" is used, with the volume fraction defined as the area ratio between the actual cross-section and its rectangular bounding box, such that

$$[C] = \frac{A_{tow}}{A_{2x1\,subcell}}\left[C_{yarn}\right] \tag{3}$$

where C_{yarn} is the result from Equation (2) and the area ratio can be found from micrograph images of the tow cross-section.

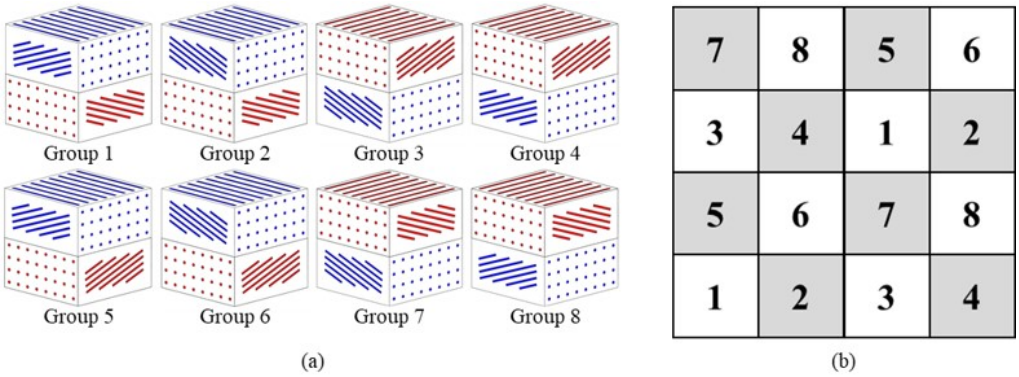

Figure 3.—(a) Unique Through-the-thickness Groups and (b) Intermediate Repeating Unit Cell.

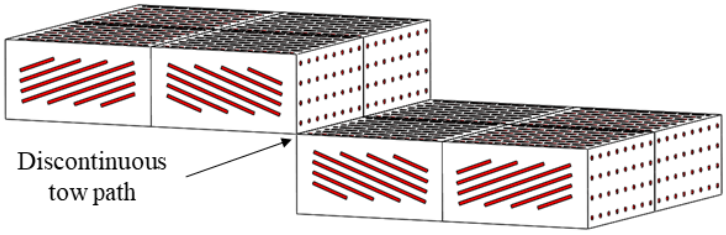

Figure 4.—Discontinuous Tow Path in the RUC.

Coordinate Transformations

In its current formulation, NASMAT assumes infinitesimal strain, which holds true in the linear-elastic regime. However, the ability of the yarns to rotate under loading due to the lack of reinforcement causes nonlinearity in the material's global response. It is therefore necessary to capture finite rotations in NASMAT and to define transformations between the local yarn and global coordinate systems. For an arbitrary off-axis loading direction, the global coordinate system, defined by the orthonormal basis $\{\mathbf{e_i^G}\}$, is such that the x-axis is aligned with the direction of loading (Figure 5(a)). The orientation of the undeformed fabric, defined by the orthonormal basis $\{\mathbf{e_i^M}\}$, in the global coordinate system is given by the off-axis angle η, such that the in-plane strains and stresses in the material coordinate system can be found from those in the global coordinate system by

$$\begin{Bmatrix} \sigma_{11}^M \\ \sigma_{22}^M \\ \tau_{12}^M \end{Bmatrix} = [Q] \begin{Bmatrix} \sigma_{xx}^G \\ \sigma_{yy}^G \\ \tau_{xy}^G \end{Bmatrix} \text{and} \begin{Bmatrix} \varepsilon_{11}^M \\ \varepsilon_{22}^M \\ \varepsilon_{12}^M \end{Bmatrix} = [Q] \begin{Bmatrix} \varepsilon_{xx}^G \\ \varepsilon_{yy}^G \\ \varepsilon_{xy}^G \end{Bmatrix} \tag{4}$$

$$Q = \begin{bmatrix} \cos^2(-\eta) & \sin^2(-\eta) & 2\cos(-\eta)\sin(-\eta) \\ \sin^2(-\eta) & \cos^2(-\eta) & -2\cos(-\eta)\sin(-\eta) \\ -\cos(-\eta)\sin(-\eta) & \cos(-\eta)\sin(-\eta) & \cos^2(-\eta) - \sin^2(-\eta) \end{bmatrix} \tag{5}$$

The local coordinate system, given by the arbitrary basis $\{\mathbf{e_i^L}\}$, is defined such that the 1-axis is aligned with the warp yarn and the 2-axis is aligned with weft yarn. In the material's undeformed state, the local and material coordinate systems are aligned. As the tows rotate relative to one another, the warp and weft yarns are no longer orthogonal, and therefore to determine the local axial strains a nonorthogonal coordinate system transformation is needed (Figure 5(b)). In each coordinate system the 3-axis remains constant and is thus excluded from Figure 5.

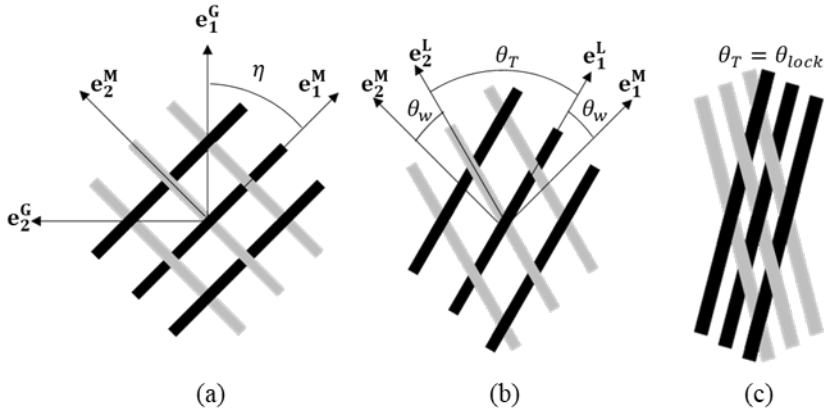

Figure 5.—(a) Transformation from Global to Material Coordinate System, (b) Transformation from Material to Local Coordinate System and (c) Schematic of Fabric at Locking Angle.

Peng et al. developed a relationship between incremental in-plane strain and stress in the material, and local coordinate systems based on the rotation of the two tows (Ref. 19), utilized here as

$$\begin{Bmatrix} \Delta\sigma_{11}^{L} \\ \Delta\sigma_{22}^{L} \\ \Delta\tau_{12}^{L} \end{Bmatrix} = [T] \begin{Bmatrix} \Delta\sigma_{11}^{M} \\ \Delta\sigma_{22}^{M} \\ \Delta\tau_{12}^{M} \end{Bmatrix} \text{and} \begin{Bmatrix} \Delta\varepsilon_{11}^{L} \\ \Delta\varepsilon_{22}^{L} \\ \Delta\varepsilon_{12}^{L} \end{Bmatrix} = [T] \begin{Bmatrix} \Delta\varepsilon_{11}^{M} \\ \Delta\varepsilon_{22}^{M} \\ \Delta\varepsilon_{12}^{L} \end{Bmatrix} \tag{6}$$

$$T = \begin{bmatrix} \cos^2\theta_w & \sin^2\theta_w & \sin\theta_w\cos\theta_w \\ \cos^2(\theta_T+\theta_w) & \sin^2(\theta_T+\theta_w) & \sin(\theta_T+\theta_w)\cos(\theta_T+\theta_w) \\ 2\cos\theta_w\cos(\theta_T+\theta_w) & 2\sin\theta_w\sin(\theta_T+\theta_w) & \sin(2\theta_w+\theta_T) \end{bmatrix} \tag{7}$$

note that in Equations (4) and (6), tensorial shear strain is used. This approach provides a procedure for relating globally applied loads to local axial strains in the warp and weft yarns. In the local coordinate system, only axial strains are used to determine updated material properties. The tows can rotate relative to one another until the locking angle is reached, in which the pores between the warp and weft yarns are closed and the yarns can no longer physically rotate any further (Figure 5(c)).

Determination of Defining Angles

Because a textile fabric is unreinforced by a matrix, the tows are free to change shape and orientation when loaded. In order to accurately model fabric behavior, the multiscale code needs to have procedures to update the crimp and rotation angles of the tows as a function of the applied loading. The crimp angle ϕ has been shown to change with axial tension in the warp or weft direction (Refs. 7, 20, and 21). When considering the stress-strain curve of a fabric subject to an applied load in either the warp or weft direction, four regions are present (Figure 6) (Ref. 20). The first region is characterized by low initial stiffness followed by nonlinear behavior, in which the yarn in the loading direction is straightened and the yarn in the transverse direction increases in crimp. This process, called crimp interchange, continues until the loading yarn is completely straightened or the transverse yarn reaches a jamming state (Ref. 21). The second region is characterized by linear-elastic behavior due to the constant crimp in both yarns throughout the region. In the third region, nonlinear behavior is attributed to failure of individual fibers within the longitudinal yarns (Ref. 20). As individual fibers fail the load carrying capacity of the fabric decreases until ultimate failure is reached in region four.

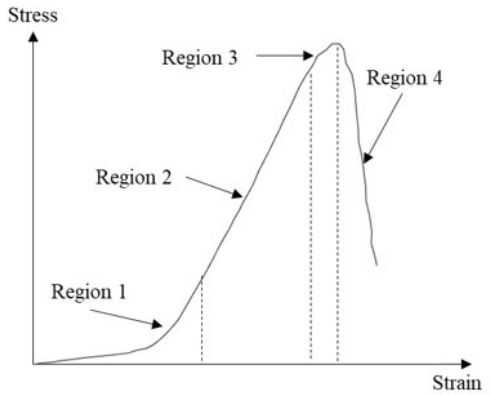

Figure 6.—Typical Fabric Stress-Strain Curve for Uniaxial Tension.

In this work, the crimp angle is assumed to vary linearly with local axial strain, such that

$$\phi_{warp} = \phi_{warp,0} + b\left(\varepsilon_{22}^{L} - \varepsilon_{11}^{L}\right) \tag{8}$$

$$\phi_{weft} = \phi_{weft,0} + b\left(\varepsilon_{11}^{L} - \varepsilon_{22}^{L}\right) \tag{9}$$

where ϕ_0 is the undeformed crimp angle, ε_{11}^{L} and ε_{22}^{L} are the local axial strains, and b is a material constant. For a uniaxial tensile load, if the loading yarn's crimp angle is calculated to be equal or less than zero, then its value is set to zero and the other is held at its current value for the remainder of the analysis.

Tows within a fabric will rotate relative to one another when subject to an off-axis load. Previous work in modeling the off-axis response of fabrics has shown that the angle between tows is well represented by ideal pin-joint kinematics (Refs. 8, 22, 23, and 24). For a general off-axis angle between the direction of loading and the warp yarn, η, the angle between the tows θ_T can be found from

$$\theta_T = 90^\circ - \left[2\psi - 2\cos^{-1}\left(\cos(\psi) + \frac{\varepsilon_N}{2\cos(\psi)}\right)\right] \tag{10}$$

$$\psi = 45^\circ - |\eta - 45| \tag{11}$$

where ψ is a parameter used to treat complimentary angles as equal and ε_N is the normalized displacement in the form of strain (Ref. 25). For coupon fabric samples

$$\varepsilon_N = \frac{\delta}{L - W} \tag{12}$$

where δ is displacement, L is the sample length and W is the sample width. The individual tow rotation angles for the warp and weft yarns are then defined as

$$\theta_{warp} = \left(90^\circ - \theta_T\right)\sin^2(\eta) \tag{13}$$

$$\theta_{weft} = -\left(90^\circ - \theta_T\right)\cos^2(\eta) \tag{14}$$

Relative rotation of the tows allows the fabric to globally experience large deformation. However, at the mesoscale the tows experience relatively low strains and finite rotations. Therefore, the small strain assumptions used in the original GMC homogenization procedure is valid and can be used for unreinforced textile fabrics.

Tow Friction

For a fabric subject to an off-axis tensile load, the force-displacement curve can be broken into three distinct regions (Figure 7). In the first region, the tows primarily rotate relative to one another at cross-over points, resulting in a low force-displacement response due to friction dominating the behavior of the fabric. Once a critical angle (θ_{cr}) is achieved and the yarns become tightly packed, the stiffness increases

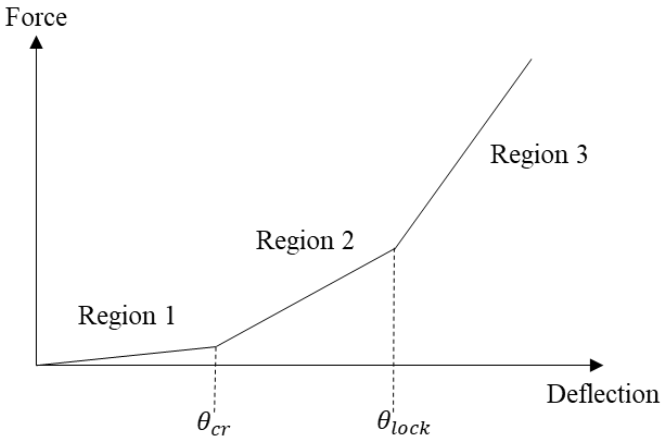

Figure 7.—Typical Force-Deflection Curve for a Fabric Subject to Off-Axis Tension.

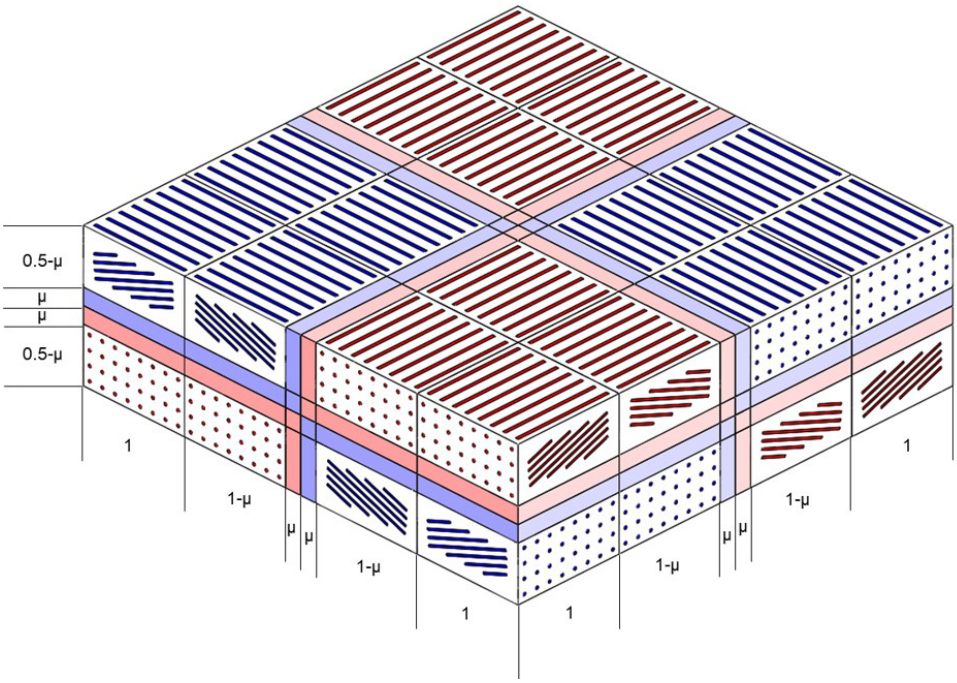

Figure 8.—Fabric RUC with Friction Interfaces.

as both rotation and sliding occurs between yarns. The yarns continue to rotate until they reach the material's locking angle (θ_{lock}), in which yarns can no longer rotate relative to one another and yarn sliding dominates the behavior (Ref. 26).

To account for the frictional interactions that occur between tows in the RUC, interfacial subcells are added at each warp and weft subcell interface in the RUC in both the vertical and horizontal planes (Figure 8). At each interface, two subcells used to represent friction are added between real material subcells, shown in Figure 9, such that the effects of friction can be accounted for independently for the warp and weft yarns. Throughout an analysis, interface subcell widths remain fixed, and are sized such that the dimensions of a subcell and its interfaces is equal to that of the subcells in Figure 2. As the subcell width μ approaches zero, the dimensions of each subcell in the new RUC approach those of the original RUC.

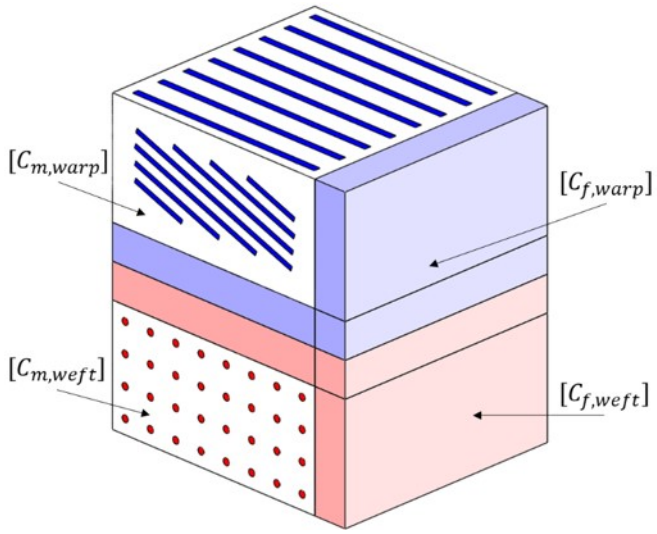

Figure 9.—Example Through-thickness Group with Interfacial Subcells.

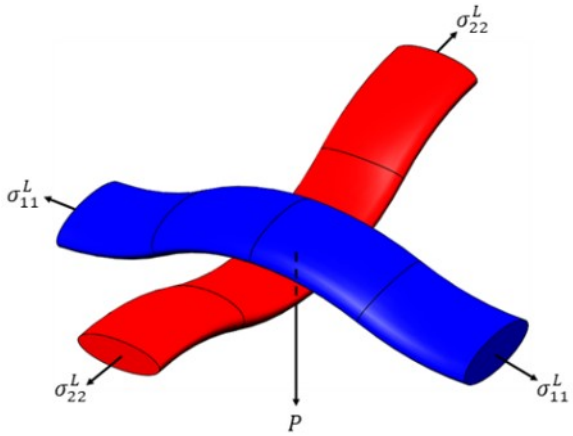

Figure 10.—Schematics of Tow Cross-Over Pressure.

The material properties assigned to the interfacial subcells range between a minimal, near-zero stiffness isotropic material and the adjacent real material, scaled such that

$$\left[C_f\right] = g\left[C_m\right] + \left(1-g\right)\left[C_{f0}\right] \tag{15}$$

where C_{f0} is the minimal stiffness matrix, C_m is the actual material stiffness matrix, and C_f is the interfacial subcell stiffness matrix. The parameter g ranges between 0 and 1 and is an effective measure of how dominant a role friction plays at the cross-over points for a given state of loading. In order to relate the interface stiffness scaling parameter g to the physical phenomena that occur during loading, it was chosen to vary with the state of contact between tows at the cross-over points. Pan et al. (Ref. 27) showed that for a plain woven fabric the normal cross-over pressure between tows due to in-plane loading (Figure 10) can be incrementally calculated at each load step as

$$P = 2\sigma_{11}^{L}\sin\phi_{warp} + 2\sigma_{22}^{L}\sin\phi_{weft} \tag{16}$$

in which axial stresses are expressed in the local, nonorthogonal coordinate system.

The state of contact between warp and weft tows is described by simplified version of the Hertzian contact theory, which has been widely used in the literature to model contact between individual fibers in unreinforced textile fabrics (Refs. 1, 28, 29, and 30). For simplicity, each tow is assumed to be spherical such that the contact area is a circle whose radius is given by

$$a_c = \sqrt[3]{\frac{6F\left(\frac{1}{E_T}\right)}{4\left(\frac{1}{R_{warp}}+\frac{1}{R_{weft}}\right)}} \tag{17}$$

where R_{warp} and R_{weft} are the representative radius of each tow and F is the contact force, given as a function of cross-over pressure as

$$P = \frac{3F}{2\pi a_c^2} \tag{18}$$

The parameter g is a function of the contact are between tows and must be normalized between 0 and 1. A maximum contact radius is therefore needed such that g can be prescribed as

$$g = \frac{\pi a_c^2}{\pi a_{c,max}^2} \tag{19}$$

The maximum contact radius is defined by the compressive displacement required to increase to tow volume fraction to 1 (Figure 11). Tows areas are assumed to be lenticular with each lens half radius remaining constant throughout the loading. Displacement is assumed to only change the distance between each lens half, thus reducing the area of the tow. The area of each tow as a function of the contact displacement is therefore given by

$$A_{tow} = r_1^2 \cos^{-1}\left(\frac{d^2+r_1^2-r_2^2}{2dr_1}\right) + r_2^2 \cos^{-1}\left(\frac{d^2+r_2^2-r_1^2}{2dr_2}\right) \tag{20}$$

where r_1 and r_2 are the radius of each lens half, d is the distance between lens half centers, and Δ is given by

$$\Delta = \frac{1}{4}\sqrt{(-d+r_1+r_2)(d-r_1+r_2)(d+r_1-r_2)(d+r_1+r_2)} \tag{21}$$

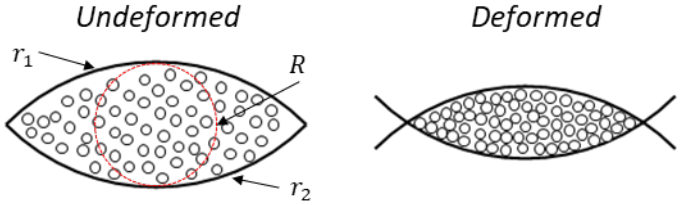

Figure 11.—Assumed Deformation of Tow from Cross-Over Pressure.

The distance between lens centers is the sum of undeformed center-to-center distance, d_0, and the Hertzian displacement, δ, such that

$$d = d_0 + \delta \tag{22}$$

where

$$\delta = \frac{a_c^2}{R} \tag{23}$$

and

$$\frac{1}{R} = \frac{1}{R_{warp}} + \frac{1}{R_{weft}} \tag{24}$$

Substituting Equations (23) into Equation (20), the maximum contact radius used in Equation (19) can be solved for by setting the left hand side of Equation (20) to the product of the original volume fraction and tow area, $V_{f,0} \cdot A_0$.

The relative width of the interface subcells, μ, is a function of the off-axis loading angle, η. μ was chosen to be expressed as a percentage of the original subcell dimension and is a measure of how dominant a role friction plays in the fabric response before the tows begin to rotate and align with the direction of loading. The largest value of μ are associated with the 45° off-axis loading case, while the smallest are associated with the unidirectional cases.

Introduction of the interface subcells requires an updated homogenization procedure for the RUC. Because each of the original eight through-the-thickness groups will have corresponding interfaces, the new intermediate RUC is represented by six subcells in the warp and weft directions, one in the thickness direction, and features 16 unique groups. The new intermediate RUC group definitions and numbering can be seen in Figure 12. In Figure 12(a), U and D indicate whether the fibers are pointed up or down, 1 and 2 refer to the direction the fibers are oriented (i.e., warp or weft), and I is used to indicate an interface subcell.

D2 D2I D1I D1	D2 D2I U1I U1	D2I D2I U1I U1I	U1I U1I U2I U2I	U1 U1I U2I U2	D1 D1I U2I U2
U2 U2I D1I D1	U2 U2I U1I U1	U2I U2I U1I U1I	U1I U1I D2I D2I	U1 U1I D2I D2	D1 D1I D2I D2
U2I (x2) D1I (x2)	U2I (x2) U1I (x2)	U2I (x2) U1I (x2)	U1I (x2) D2I (x2)	U1I (x2) D2I (x2)	D1I (x2) D2I (x2)
U1I (x2) U2I (x2)	D1I (x2) U2I (x2)	D1I (x2) U2I (x2)	D2I (x2) D1I (x2)	D2I (x2) D1I (x2)	D2I (x2) U1I (x2)
U1 U1I U2I U2	D1 D1I U2I U2	D1I D1I U2I U2I	D2I D2I D1I D1I	D2 D2I D1I D1	D2 D2I U1I U1
U1 U1I D2I D2	D1 D1I D2I D2	D1I D1I D2I D2I	U2I U2I D1I D1I	U2 U2I D1I D1	U2 U2I U1I U1

(a)

7	8	14	13	5	6
3	4	15	16	1	2
10	15	15	16	16	9
13	11	11	12	12	14
5	6	11	12	7	8
1	2	9	10	3	4

(b)

Figure 12.—(a) Through-the-thickness Group Definitions and (b) Numbering for the Fabric RUC with Frictional Interface Subcells.

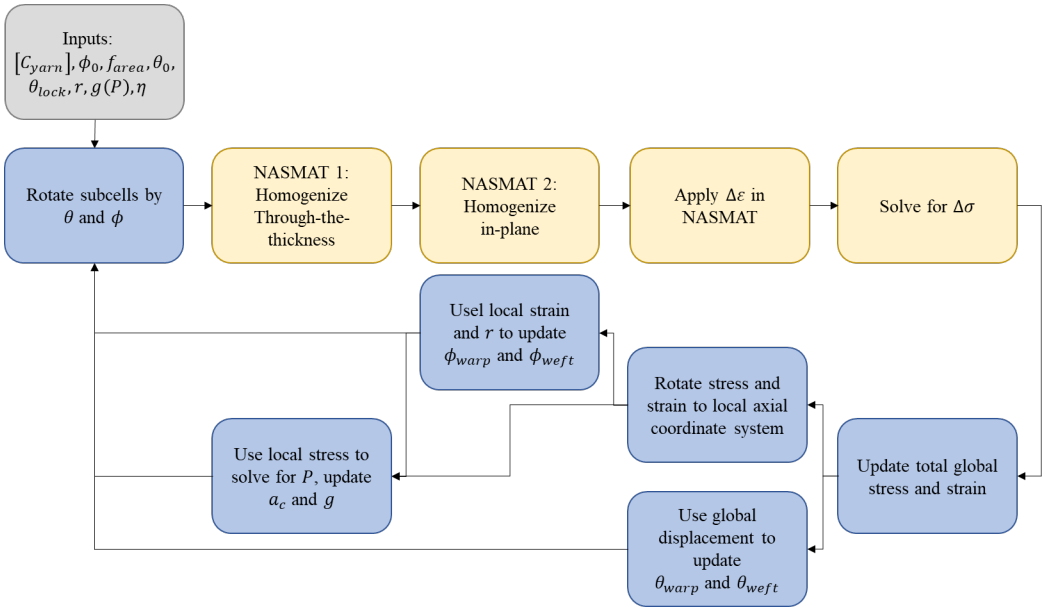

Figure 13.—Solution Procedure.

Solution Procedure

Solutions of uniaxial tension in the warp and weft directions and off-axis tension were found using NASMAT for an applied quasi-static displacement incrementally, such that the homogenized stiffness matrix of the fabric could be updated by accounting for the new tow angles at each load step. Future work will focus on integrating the tow rotations directly into the code, streamlining this process. A general procedure for the solution of the stress-strain curve for an arbitrary loading direction is outlined in Figure 13.

Results

Initialization of RUC

Experimental data for a Kevlar K706 Style Fabric (Ref. 7), which features Kevlar KM2 yarns, is used to verify the ability of the amended NASMAT code to reproduce the nonlinear response of textile fabrics. The specific weave of Kevlar was chosen due to the abundance of information available in the literature. Experimental results taken from the literature of KM2 yarn tensile tests provided the axial modulus, whose average value was 76.652 GPa. The transverse and shear moduli values were chosen to be roughly two and three orders of magnitude less than the axial modulus (500 and 80 MPa, respectively) in order to represent the low transverse stiffness and minimal shear resistance exhibited by yarns (Ref. 6). To decouple directional loading, the Poisson's ratios are all set to zero. This simulates the spreading of fibers within a tow under axial loading without the development of lateral strain (Ref. 6). A summary of the material properties used in defining the yarn compliance matrix in Equation (1) is found in Table 1.

The initial crimp angles ϕ_0 were determined from micrograph images supplied by Reference 6 of the K706 fabric (Figure 14), and were found to be 14° for the warp yarn and 9.5° for the weft yarn. The area ratio used in Equation (3) was determined to be 0.61. The rate at which the crimp angle changes, r, calibrated against the experimental data and determined to be 428°/strain.

The geometric parameters required for determining the parameter g were also found from the micrograph images supplied by Reference 6, and are summarized in Table 2. The original volume fraction of the tows was taken to be 0.907, taken from Reference 1.

TABLE 1.—SUMMARY OF KEVLAR KM2 YARN MATERIAL PROPERTIES

Property	Value	Units
E_A	766.52	GPa
E_T	500	MPa
G_{12}, G_{13}, G_{23}	80	MPa
$\nu_{12}, \nu_{13}, \nu_{23}, \nu_{21}, \nu_{31}\nu_{32}$	0	------

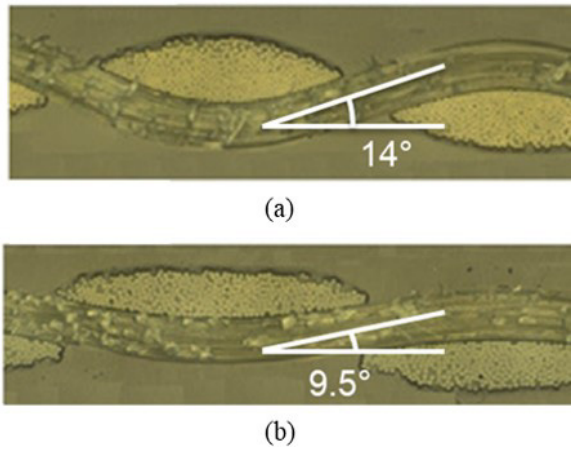

Figure 14.—(a) Warp and (b) Weft Micrograph Images of K706 Fabric with Measured Crimp Angle $\boldsymbol{\phi}$ Reference 6.

TABLE 2.—KM2 TOW GEOMETRY

Parameter	Warp	Weft
R	0.081 mm	0.063 mm
r_1	0.225 mm	0.528 mm
r_2	0.214 mm	0.768 mm
d	0.388 mm	1.239 mm
A_0	0.906E-2 mm^2	1.451E-2 mm^2

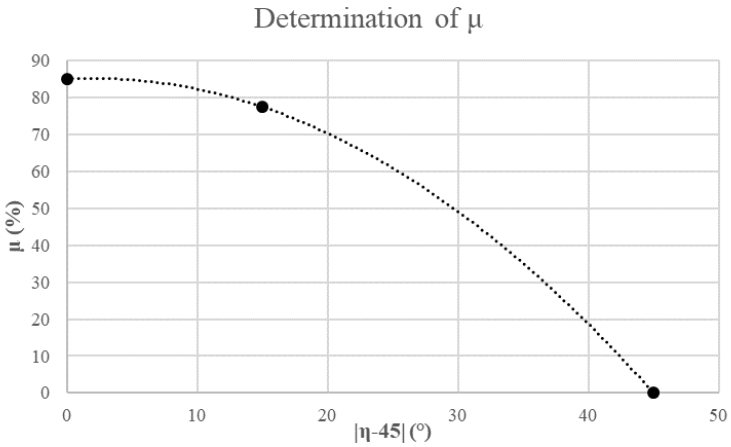

Figure 15.—Determination of $\boldsymbol{\mu}$.

The values of μ for each load case are shown in Figure 15. A quadratic curve was fit to the values that could be used for the prediction of an arbitrary off-axis loading angle, though further experimental data is required for validation.

Single Fabric RUC

NASMAT analysis was conducted for uniaxial tension in both the warp and weft direction and off-axis tension at 45° and 30° orientations. Results from NASMAT for uniaxial tension, compared to experimental results taken from Reference 7, are shown below in Figure 16, with the transition between regions 1 and 2 from Figure 6 indicated with circle markers, and NASMAT calculations for off-axis tension are shown below in Figure 17.

For each load case simulated using the RUC analysis, excellent agreement is observed between simulations and the experimental data. For uniaxial tension, the results indicate that the low stiffness and following nonlinear behavior observed in region 1 of Figure 6 can be modeled using NASMAT with a defined relationship between crimp angle and axial strain, and that the transition between regions one and two can be modeled by imposing the end condition of the crimp interchange process into the RUC subcell definition. They further showed that a linear change with respect to strain for the crimp interchange process is sufficient in capturing the overall fabric uniaxial behavior. Figure 17 shows the simulation results for the off-axis tension cases both with and without including the interface subcells in the RUC.

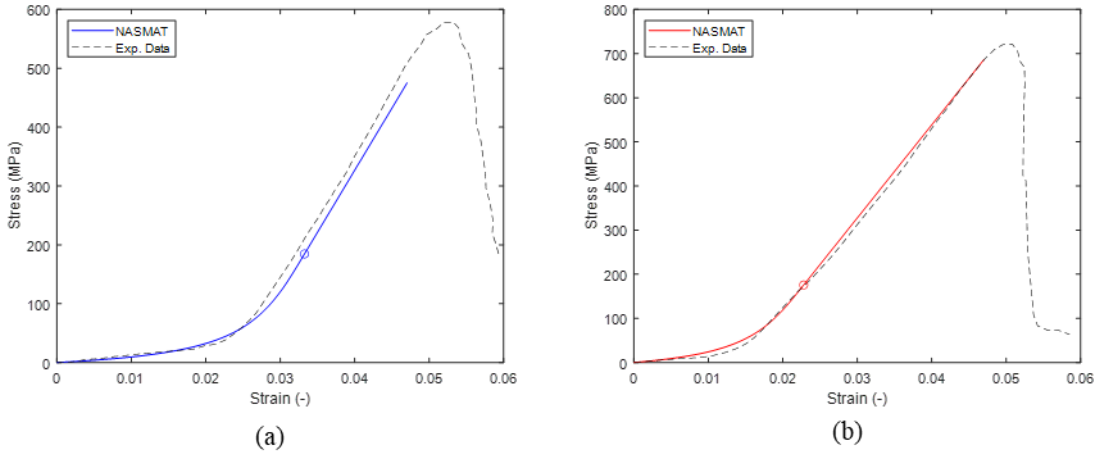

Figure 16.—NASMAT RUC Simulation of Uniaxial Tension in the (a) Warp and (b) Weft Directions.

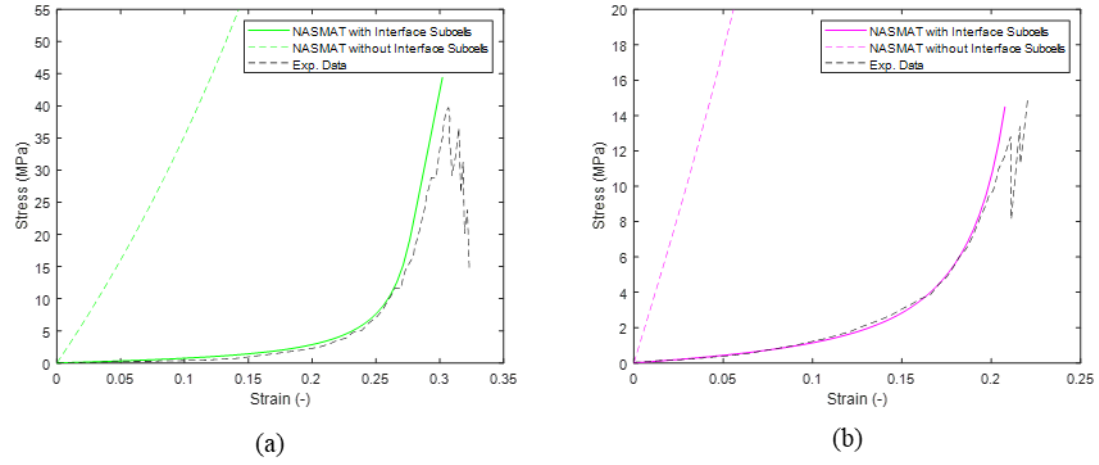

Figure 17.—NASMAT RUC Simulation of (a) 45° and (b) 30° Off-Axis Tension with and without Interface Subcells.

The results show the importance of including the interface subcells in capturing the initial low stiffness response of the fabric as the tows rotate relative to one another in order to effectively capture the contact mechanics and friction dominant behavior occurring at the cross-over points between tows that is lost in the homogenization process. The simulation results with interface subcells align well with the experimental data up until the end of the simulation, where the curve begins to deviate from the experimental data, proving to be over-stiff. This difference in response is attributed to the model's inability to predict failure in this region, where individual fibers in the warp and weft yarns are breaking, reducing the overall stiffness response of the fabric prior to a load drop.

Conclusions and Future Work

The NASMAT analysis tool developed at the NASA Glenn Research Center has been previously shown to effectively simulate the behavior of composite materials, including modeling nonlinear behavior and damage in a time efficient manner, but has been limited to reinforced fabric structures. In this work, the NASMAT code has been applied to unreinforced textile fabrics. Adaptations to the code involved allowing for the crimp of the warp and weft yarns to change with applied loading, as well as accounting for tow rotations and their relative interactions in the homogenization procedure. Compared to experimental data for Kevlar K706 fabric available in the literature, excellent correlation is observed for the NASMAT results for both uniaxial and off-axis tensile cases. The objective of this work was to determine the feasibility of using the existing tool for unreinforced textile fabrics. The results have confirmed that with the proper modifications to the existing framework, NASMAT can be used to predict fabric behavior.

The current methodology for predicting fabric behavior requires iterative calculations using NASMAT, with each iteration allowing for a change in the defining angles of the RUC run through a MATLAB (MathWorks) script. With a suitable method found for predicting fabric behavior, the next step is to implement the present work into the code's framework itself, removing the need for the controlling MATLAB script for ease of use. Other future work includes pairing the multiscale tool with the commercial finite element software Abaqus to model more complex loading scenarios, including modeling the full-field off-axis tension response and quasi-static indentation. Additional experimental data, including off-axis tension testing from angles ranging from 0° to 90° and data from different materials will also aid in the overall development of the amended code, and can provide additional information and insight on the determination of the parameters used in this work that were determined experimentally. Finally, the ability to calculate permeability of fabrics based on porosities between warp and weft yarns and between yarns themselves will be added to the present code structure, which is a critical factor when considering parachute response. Development of permeability into the NASMAT code will include experimental characterization of the porosity, or ratio of fabric to open space, and the permeability, or rate of flow of air through the fabric, and appropriate adaptation of the RUC to predict airflow through a fabric. Ultimately, the analysis tool will be sufficiently developed to be paired with fluid-structure interaction solvers to predict the behavior and failure of parachute deployment systems.

References

1. S. Sockalingam, J.W. Gillespie Jr. and M. Keefe, "Modeling the Transverse Compression Response of Kevlar KM2," *American Society of Composites Conference*, pp. 749–766, 2013.
2. R. Samadi and F. Robitaille, "Particle-based modeling of the compaction of fiber yarns and woven textiles," *Textile Research Journal*, vol. 84, no. 11, pp. 1159–1173, 2014.

3. M. Grujicic, A. Hariharan, B. Pandurangan, C.F. Yen, B.A. Cheeseman, Y. Wang, Y. Miao and J.Q. Zheng, "Fiber-Level Modeling of Dynamic Strength of Kevlar KM2 Ballistic Fabric," *Journal of Materials Engineering and Performance*, vol. 21, no. 7, pp. 1107–1119, 2012.
4. Y. Duan, M. Keefe, T. Bogetti and B. Powers, "Finite element modeling of transverse impact on a ballistic fabric," *International Journal of Mechanical Sciences*, vol. 48, no. 1, pp. 33–43, 2006.
5. E. Barbero, J. Trovillion, J. Mayugo and K. Sikkil, "Finite element modeling of plain weave fabrics from photomicrograph measurements," *Composite Structures*, vol. 73, no. 1, pp. 41–52, 2006.
6. G. Nilakantan, S. Horner, V. Halls and J. Zheng, "Virtual ballistic impact testing of Kevlar soft armor: Predicitve and validated finite element modeling of the V0-V100 probabilistic penetration response," *Defence Technology*, vol. 14, pp. 213–225, 2018.
7. Z. Dong, J. Manimala and C.T. Sun, "Mechanical Behavior of Silica Nanoparticle-impregnated Kevlar Fabrics," *Journal of Mechanics of Materials and Structures,* vol. 5, no. 4, pp. 529–548, 2010.
8. O. Erol, B. Powers and M. Keefe, "Development of non-orthogonal macroscale material model for advanced woven fabrics based on mesoscale structure," *Composite Part B*, vol. 110, pp. 497–510, 2017.
9. G. Nilkantan, M. Keefe, T. Bogetti, R. Adkinson and J. Gillespie, "On the finite element analysis of woven fabric impact using multiscale modeling techniques," *International Journal of Solids and Structures*, vol. 47, no. 17, pp. 2300–2315, 2010.
10. I. Verpoest and S. Lomov, "Virtual textile composites software WiseTex: Integration with micro-mechanical, permeability and structural analysis," *Composites Science and Technology*, vol. 65, pp. 2563–2574, 2005.
11. S. Lomov V.D. Ivanov S.I. Verpoest, M. Zako, T. Kurashiki, H. Nakai and S. Hirosawa, "Meso-FE modelling of textile composites: Road map, data flow and algorithms," *Compistes Science and Technology*, vol. 67, pp. 1870–1891, 2007.
12. B. Bednarcyk, "Modeling Woven Polymer Matrix Composites with MAC/GMC," *NASA Contractor Report*, pp. 1–20, 2000.
13. B. Bednarcyk and S. Arnold, "Micromechanics-based deformation and failure prediction for longitudinally reinforced titanium composites," *Composites Science and Technology*, vol. 61, pp. 705–729, 2001.
14. T. Ricks, B. Farrokh, B. Bednarcyk, and E. Pineda, "A Comparison of Different Modeling Strategies for Predicting Effective Properties of 3D Woven Composites," *AIAA SciTech Forum*, pp. 1–11, 2019.
15. Liu, K. and Chattopadhyay, A. and Bednarcyk, B. and Arnold, S.M., "Efficient Multiscale Modeling Framework For Triaxially Braided Composites using Generalized Method of Cells," Journal of Aerospace Engineering, 2011.
16. J. Aboudi, "Micromechanical Analysis of Thermo-Inelastic Multiphase short-Fiber Composites," *Composites Engineering*, vol. 5, no. 7, pp. 839–850, 1995.
17. Bednarcyk, B.A., and S.M. Arnold. 2003. "Micromechanics-based modeling of woven polymer matrix composites," AIAA J., 41(9), pp. 1788–1796.
18. B. Bednarcyk and S. Arnold, "MAC/GMC 4.0 User's Manual - Example Problem Manual," NASA/TM—2002-212077/VOL3, pp. 1–284, 2002.
19. X.Q. Peng and J. Cao, "A continuum mechanics-based non-orthogonal constitutive model for woven composite fabrics," *Composites: Part A*, vol. 36, pp. 859–874, 2005.
20. D. Zhu, B. Mobasher, J. Erni, S. Bansal and S.D. Rajan, "Strain rate and gage length effects on tensile behavior of Kevlar 49 single yarn," *Composites: Part A,* vol. 43, pp. 2021–2029, 2012.
21. P. Potluri and V.S. Thammandra, "Influence of uniaxial and biaxial tension on meso-scale geometry and strain fields in a woven composite," *Composite Structures*, vol. 77, pp. 405–418, 2007.

22. P. Boisse, N. Hamila, E. Guzman-Maldonado, G. Anglea Madeo and F. Dell'Isola, “The bias-extension test for the analysis of in-plane shear properties of textile composite reinforcements and prepregrs: a review,” *International Journal of Material Forming*, vol. 10, no. 4, pp. 473–492, 2017.
23. P. Harrison, F. Abdiwi, Z. Guo, P. Potluri and W. R. Yu, “Characterising the shear-tension coupling and wrinkling behaviour of woven engineering fabrics,” *Composites: Part A*, vol. 43, pp. 93–914, 2012.
24. P. Harrison, M.F. Alvarez and D. Anderson, “Towards comprehensice charachterisation and modelling of the forming and wrinkling mechanics of engineering fabrics,” *International Journal of Solids and Structures*, vol. 154, pp. 2–18, 2018.
25. A. Milani, J. Nemes, G. Lebrun, M. Bureau, “A Comparative Analysis of a Modified Picture Frame Test for Characterization of Woven Fabrics,” *Polymer Composites*, vol. 21, no. 4, pp. 561–568, 2010.
26. J. Domskienė and E. Strazdienė, “Investigation of Fabric Shear Behavior,” *Fibres & Textiles in Eastern Europe*, vol. 13, no. 2, pp. 26–30, 2005.
27. N. Pan, “Analysis of woven fabric strengths: prediction of fabric strength under uniaxial and biaxial extensions,” *Composite Science and Technology*, vol. 56, pp. 311–327, 1996.
28. S. Sockalingam, R. Bremble, J.W. Gillespie Jr. and M. Keefe, “Transverse compression behavior of Kevlar KM2 single fiber,” Composites Part A, vol. 81, pp. 271–281, 2016.
29. S. Kawabata, “Measurement of the Transverse Mechanical Properties of High-performance Fibres,” Journal of the Textile Institute, vol. 81, no. 4, pp. 432–447, 1990.
30. J. Singletary, H. Davis, M.K. Ramasubramanian, W. Knoff and M. Toney, “The transverse compression of PPTA fibers,” Journal of Materials Science, vol. 35, pp. 573–581, 2000.